



Characterization of an Unstable Slope Using Geophysical, UAV, and Geological Techniques: Karakoram Himalaya, Northern Pakistan

Muhammad Younis Khan^{1*}, Muhammad Shafique^{1,2}, Syed Ali Turab¹ and Naseem Ahmad^{1,2}

¹National Centre of Excellence in Geology, University of Peshawar, Peshawar, Pakistan, ²GIS and Space Application in Geosciences (GSAG) Lab, National Centre of GIS and Space Applications, Institute of Space Technology, Peshawar, Pakistan

Given active tectonism, rough terrain, and climate, the mountainous ranges in northern Pakistan are prone to geohazards, including earthquakes, unstable slopes, and landslides. The frequent landsliding in the region poses a risk to communities, economic activities, and transportation networks. In this context, the unstable slope above Mayun village calls for a multi-method approach for better assessment of the slope for planning interventions aimed at hazard mitigation. We conducted an integrated study including uncrewed aerial vehicle (UAV) and ground-penetrating radar (GPR) in coordination with geomorphic field observations to image the possible slip surfaces for a comprehensive understanding of a potential future rockslide with significant socioeconomic consequences. UAV-derived results helped delineate the overall extent of the unstable slope and its downslope area in a quick, remote, and safe way. GPR profiles have enabled the reconstruction of the bedrock's morphology and its internal structure and the depth distribution of cracks running through the overburden and bedrock. The results provided insight into the stable and unstable compartments of the slope due to the thin cover of surficial deposits, high impedance contrast at the overburden-bedrock interface, lateral heterogeneities, and presence of open cracks, and almost detached blocks, respectively. These data on the dynamic properties of a landslide-prone slope could be used for the correct planning of civil infrastructure to minimize the potential risk of building damage in the seismically active Hunza valley.

Keywords: GPR, integrated approach, unstable slope, landslide, Karakoram Himalaya

INTRODUCTION

Pakistan is considered among one of the most seismically active zones in the world due to ongoing collision between the Eurasian and Indian plates resulting in the convergence of the latter at a rate of 50 mm/year (Alvarez, 2010). Due to active tectonism, rough terrain, and climatic factors, northern Pakistan is frequently exposed to landslides and large earthquakes with devastating impacts on society and the economy (Shafique et al., 2015; Khan et al., 2021). In North Pakistan, the western Karakoram region has a remarkable history of seismicity, extreme climate, and a diverse topographical setting, such as valleys, ridges, and slopes. The Hunza valley of the western Karakoram has been known for slope instabilities (Bird and Bommer, 2004). In such a high mountain environment, slopes are considered high-risk

OPEN ACCESS

Edited by:

Simon James Cook,
University of Dundee, United Kingdom

Reviewed by:

Jan Klimes,
Institute of Rock Structure and
Mechanics (ASCR), Czechia
Joern Lauterjung,
German Research Centre for
Geosciences, Germany

*Correspondence:

Muhammad Younis Khan
myouniskhan@uop.edu.pk

Specialty section:

This article was submitted to
Geohazards and Georisks,
a section of the journal
Frontiers in Earth Science

Received: 15 February 2021

Accepted: 02 August 2021

Published: 27 August 2021

Citation:

Khan MY, Shafique M, Turab SA and
Ahmad N (2021) Characterization of an
Unstable Slope Using Geophysical,
UAV, and Geological Techniques:
Karakoram Himalaya,
Northern Pakistan.
Front. Earth Sci. 9:668011.
doi: 10.3389/feart.2021.668011

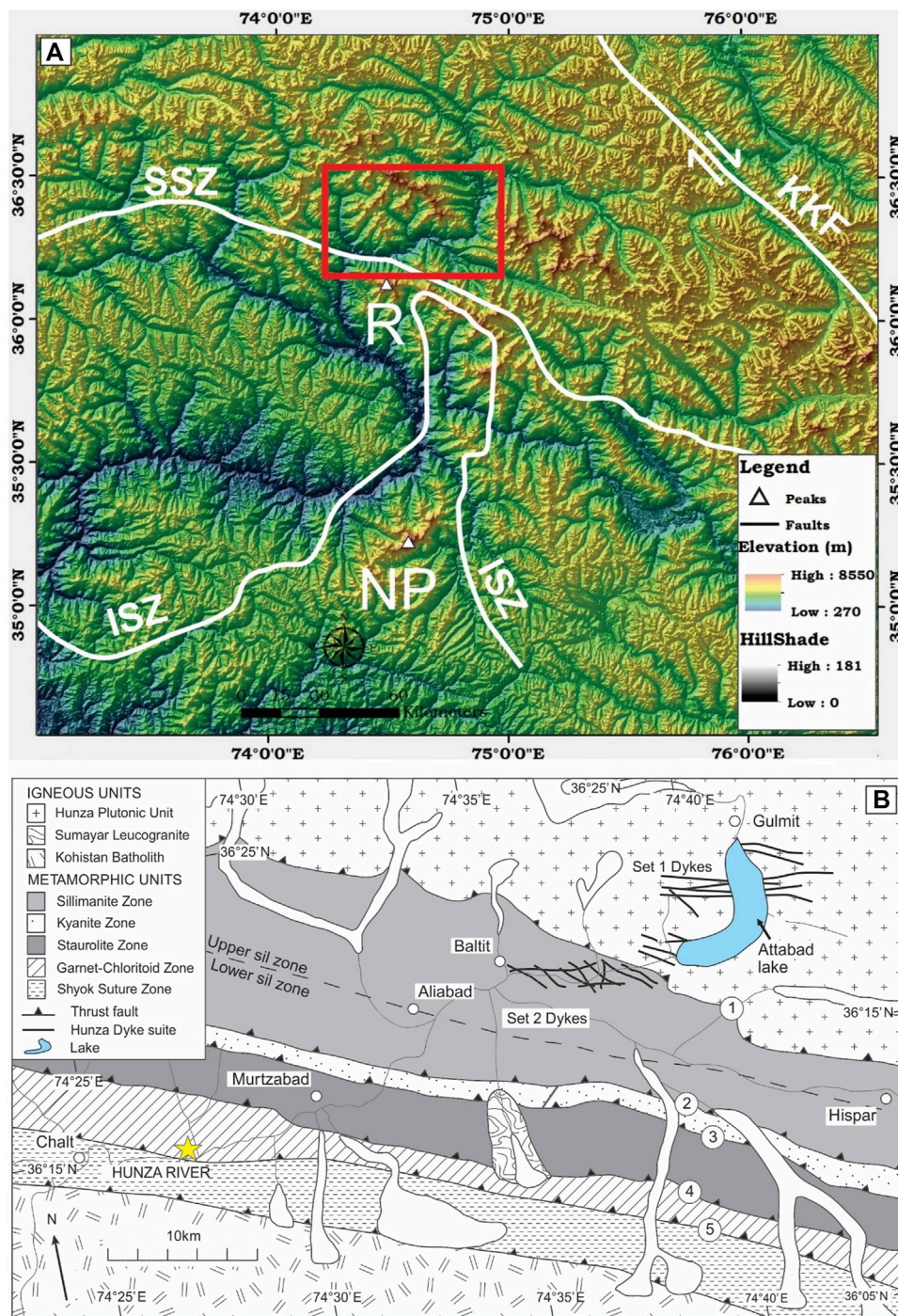


FIGURE 1 | (A) Digital Elevation Model (DEM) with shaded-relief of northern Pakistan showing the location of the major faults. The red box denotes the location of Panel 1**(B)**. ISZ: Indus Suture Zone; SSZ: Shyok Suture Zone; KKF: Karakoram Fault; NP: Nanga Parbat; R: Rakaposhi. Panel 1**(B)** geological map of the Hunza Valley showing tectonic relations. The locality of the study site is marked with a yellow star. Thrusts dividing segments of the Karakoram metamorphic complex are numbered: 1, Hunza; 2, Hassanabad; 3, North Murtzabad; 4, South Murtzabad; 5, MKT (after Palin et al., 2012).

landforms due to the occurrence of landslide processes that result in huge economic losses and human casualties. The 2010 Attabad landslide dam is the latest example in the region that claimed human lives and affected the operation of the

world's highest international highway, i.e., Karakoram Highway (KKH), by blocking the Hunza River. This study is focused on the Mayun village in the Hunza valley situated within 1 km of the main Karakoram thrust (MKT), where the

Asian plate and the Kohistan Island Arc were sutured (**Figure 1**).

Globally, rock slope failures in many mountainous areas are considered one of the major natural hazards. Thus, the identification and characterization of rock slope failure are key tasks in designing effective strategies for risk management. There are several mitigation strategies to cope with the risk, but the simplest one is to avoid construction on unstable slopes and/or adjacent to a rock slope about to collapse; however, this is not always practical for various reasons, including rapid growth in population, poverty, and availability of plain residential land in mountainous areas like the Karakoram in northern Pakistan. Therefore, the Mayun slope above the Mayun village represents a significant case study in Pakistan, owing to its location in a very complex geologic setting characterized by strong seismic activity and effects of extreme internal crustal and external surficial stresses (Chen et al., 2017). In such mountainous terrain, remote sensing techniques offer certain advantages such as high resolution and broad spatial coverage of inaccessible area over other ground-based methods (e.g., boreholes, slope inclinometers, and penetrometric tests), which provide limited information at discrete points and are expensive, time-consuming, laborious, and destructive in nature. Therefore, these technologies [Interferometric Synthetic Aperture Radar (InSAR), Light Detection and Ranging (LiDAR), and uncrewed aerial vehicle (UAV) photogrammetry] have been applied to a variety of geohazard related problems, including landslides and natural slopes (Marsella et al., 2015; Petschko et al., 2016; Fan et al., 2017; Fey and Wichmann, 2017; Roque et al., 2018). Recently, the use of UAVs as a low-cost alternative to assess slope conditions has seen much interest worldwide (Tahar, 2012; Huang et al., 2017; Ghorbanzadeh et al., 2019).

Slope failure is a complex phenomenon, a prerequisite for understanding the evaluation of internal structure by delineating interface boundaries, material inhomogeneities, and establishing overburden-bedrock contact in slope stability analyses. Surface-based geophysical methods provide high-resolution images with large spatial coverage to derive physical parameters of materials and structures. Geophysical techniques (seismic arrays, resistivity, and induced polarization) have been used to investigate slopes in various geological settings where direct measurements through borehole and trenches are not possible for various reasons (Danneels et al., 2008; Marescot et al., 2008). Among the geophysical methods, GPR has received much attention due to being lightweight, portable, high in resolution, inexpensive, time-effective, and easy to use in order to capture slope dynamics in very rough terrain such as in the Karakoram Himalaya (Toshioka et al., 1995; Deparis et al., 2007; Danneels et al., 2008). The successful applications have been largely due to the capability of its high vertical and lateral resolution. GPR allows the acquisition of information on the subsoil from the response of the materials to high-frequency electromagnetic radio waves. The signal reflected at boundaries with different dielectric constants (i.e., stratigraphic contacts, failure planes, cavities, and water table) is recorded.

To address a complex problem like slope failure, it is common to apply different methods for the same field site to take full

advantage of a multitechnique approach combining geophysics with remote sensing methods (Deparis et al., 2008; Willenberg et al., 2008). Nonetheless, this information needs to be integrated with the field observations. The Mayun slope is a typical complex site with a variable fracture network in terms of density, surface extension, and orientation. Considering that it is unstable, it poses a threat to hundreds of houses located in the downslope area and has the potential to generate a catastrophic landslide, which may subsequently block the river Hunza and the Karakoram Highway. Apart from using the KKH as a trade route, it is also the only highway available in the region for tourists, national and international skiers, and hikers to reach different spots of interest in north Pakistan. Despite its importance for local people and visitors from abroad, it is well-established that the entire north of Pakistan, and hence the study area, is exposed to a considerable natural risk.

Therefore, an integrated approach was employed to evaluate the surface features (using UAV) and the internal structure (using GPR) of the Mayun slope and accordingly suggest effective mitigation measures to reduce the risk. To the best of our knowledge, to date, no studies integrating space-, air-, and ground-based techniques with geomorphology have been conducted to study slope dynamics in the study area. Such results also have implications for the larger Himalaya-Karakoram-Hindukush (HKH) region, sharing similar climatic-geomorphic and geologic settings.

GEOLOGICAL AND TECTONIC SETTING OF THE STUDY AREA

Hunza valley is located in north Pakistan across two geological terrains, the Karakoram plate and the Kohistan Island Arc (**Figure 1**). The boundary between the two is marked by the main Karakoram thrust (MKT) and passes through the valley near Chalt. Geologically, the study site is the southern part of the Karakoram plate and the bedrock geology is dominated by metamorphic rocks that have experienced strong deformation and regional metamorphism due to the India-Asia collision (Crawford and Searle, 1993; Palin et al., 2012). Foliations associated with tectonic deformation may provide plane(s) of weakness(es) for possible rock failure. As most or all of the Karakoram had observed several episodes of glaciation in the Pleistocene (Holmes and Shroder, 1993), the glacial debuitting may have prepared slopes for failure (Ballantyne, 2002; Hewitt et al., 2011; Zabaleta et al., 2020). Driving some of the world's highest rock uplift rates are reported from the area (Zeitler, 1985), driving higher rates of denudation and erosion. Erosionally induced stresses may also contribute directly to rock sliding or by exploiting preexisting planes of weakness.

MATERIALS AND METHODS

To characterize the unstable slope, an integrated approach was adopted, details of which are provided in the following subsections.

Geomorphology

Hunza valley exhibits one of the most extreme topographies in the world, e.g., Rakaposhi, with an elevation of 7,788 m, increasing about 5,900 m from the Hunza River. The Mayun slope is at a distance of about 12 km from Rakaposhi along the northern slope of Hunza valley. Generally, the local relief is greater than 2,500 m in the entire valley. The terrain is comprised of thousands of square kilometers of the steep rock wall. Rivers tend to align parallel, or nearly so, to geological lineaments or the margins of stratigraphic and plutonic units (Seeber and Gornitz, 1983; Cronin et al., 1989). Detachment zones of rockfalls and rock slides often lie at valley junctions or directly opposite to the entrance of large tributaries (Hewitt, 2001). Geomorphic activity prevailing in the area is described as extreme by global standards, especially the work of debris flows and flood-prone rivers, rock falls and rock slides, snow avalanches, and valley glaciers (De Filippi, 1912; Goudie et al., 1984; Shroder et al., 1993).

Several geomorphic features, such as active erosional agents (the Hunza River in the downslope area, small depressions on both sides of the slope allowing glacier meltwater flow in summer, and water channel for domestic water supply), a short distance from the crustal-scale MKT, multi-scale cracks influenced by seasonal changes (freeze and thaw actions), almost detached blocks, high relief, and jointed bedrock makes this slope (study site) a unique candidate for investigation of slope dynamics in the high mountain environment.

Geomorphological Data Collection and Results

Despite advantages offered by the UAV data, aerial imagery should be integrated with field observations to precisely locate the structural features and collect quantitative measurements for slope characterization. The Mayun slope consists of heterogeneous and loose debris material, i.e., soft deposits over stiff metamorphic bedrock. The soft sedimentary cover could further be divided into two layers characterized by surficial sediments of a highly heterogeneous layer and a stratified layer, respectively (see **Figure 3I**).

Based on the observed geomorphological features along ZZ' cross-section on the Mayun slope, we have divided it into three sections (lower, middle, and upper). The latter has experienced more instabilities (e.g., large cracks, i.e., meter-scale, change in their depth, width, and associated slip) than other sections of the slope. We measured the length (L), width (W), depth (D), and azimuth (A) of three main cracks (see **Figures 2C, 3H, 4**). These parameters were L1 = 50 m, L2 = 12 m, L3 = 45; W1 = 1.2 m, W2 = 0.5 m, W3 = 0.3 m; D1 = 1.6 m, D2 = 0.8 m, D3 = 0.3 m; A1 = N76°E, A2 = N50°E, A3 = N82°E for C1, C2, and C3, respectively. A considerable decrease in the slip was noticed along the identified cracks in the downslope direction. The crack surfaces were not filled. The relatively debris-free characteristic of major cracks may indicate that the weathered material was highly mobile and flowed freely from the source across the slope. There was an increase in the width of the small (centimeter-scale) cracks in the upslope direction. Both small- and large-scale cracks

(C1, C2, and C3) were roughly oriented in an E-W direction (**Supplementary Figures S1, S5**). The upper part of the slope displayed more instabilities than other parts (middle and lower) due to a relatively steep gradient. The existence of almost detached blocks of length 15.5 m indicates the highly damaged rock mass of the slope, adding to the complicated process of estimating slope stability (see **Figure 3F**).

Uncrewed Aerial Vehicle Photogrammetry

To study the slope deformation, a UAV-based remote sensing system was employed due to its flexibility, cost-effective nature, and low risk (see **Supplementary Figure S4**). Such a remote sensing system is usually composed of a flight platform and a ground control system (Bürkle et al., 2011).

A four-rotor UAV system (Inspire-II) fitted with a Xenmuse X4 Camera with 20-megapixel resolution, a field of view (FOV) of 84°, and a focal length of F/2.8–11 was used to collect the aerial photos. The camera was carried on a set of aerial gimbals attached to the bottom of the UAV. The UAV flight was planned and controlled using the Pix4D Capture application.

UAV Data Collection and Results

The UAV survey was carried out to acquire detailed characteristics of the morphologic features in terms of intensity, orientation and lateral extension, lithological characteristics of debris, and outcropped bedrock (**Figures 2C–H**). Aerial photos were collected at an altitude of 200 m, 70% overlap, with a total mapped area of 2.83 km². In total, 405 images were collected using a double grid mission to map the overall area; however, the Mayun slope was extracted as the area of interest (AOI) using ArcGIS. The Structure from Motion (SfM) algorithm was applied using the Pix4D Mapper software to process the UAV data. The DGPS Post-Processing Kinematic (PPK) geodetic survey was carried out over the slope with 12 Ground Control Points (GCPs) for accurate image processing. The DEM was computed with a spatial resolution of 0.8 m and Root Mean Square Error (RMSE) of 0.43 m (see **Supplementary Figure S3**).

The UAV data were also used to map other important downslope features (e.g., water channel and the Hunza River shown in **Figures 2A, 3A**) that were not directly related to the Mayun slope but may have a strong indirect influence on mass movement processes. A significant change in texture and color could be detected between the water channel and its lower and upper sides. The physical properties of bare soil and rock contrast with the water channel characterized by lush vegetation; this assisted in precisely tracking the water channel. From the high-resolution UAV image, bushes, trees, and freshly weathered material could be detected directly underneath the Mayun slope and the surrounding mountain slopes. Additionally, a laterally extended fracture following the water channel's course and other similar features may indicate their active role in destabilizing the whole base of the rock body and hence the slope(s) located at high relief directly above these unstable sites (**Figures 2D,E**). The collapsed material and vegetation indicate an un-sealed water supply network which allowed a considerable amount of leakage to its surrounding material for a longer period

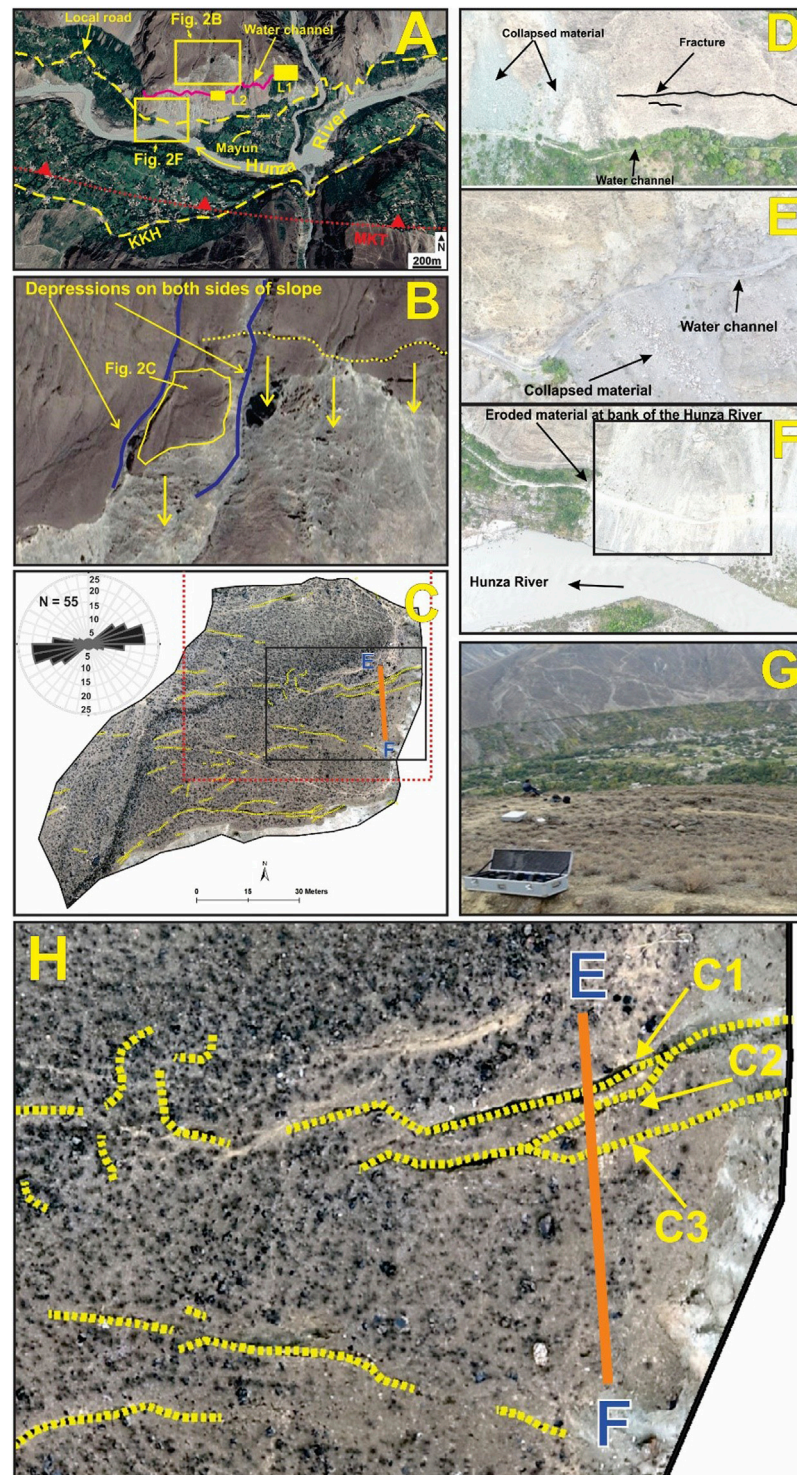


FIGURE 2 | Google Earth imagery (A,B) with larger features (MKT, KKH, local road, the Hunza River, and Mayun village) shown in Panel 2(A) and Mayun slope-specific features (its location as 2(C)); depressions denoted as solid blue lines represent depressions/tributaries, dashed-yellow line denotes the E-W oriented deformation in the upslope direction, and the solid yellow lines show the main sliding direction in Panel 2(B). Geomorphological features on UAV aerial photographs (C,D,E,F), the Mayun slope overview while standing at the crest and looking southward towards the downslope area (G), and adjacent area towards the Hunza River. Filled rectangles with yellow color (L1 and L2) in Panel 2(A) represent locations of Panels 2(D,E), respectively. In Panel 2(C), red dotted box denotes the extent of Figure 4A; solid black box represents the extent of Panel 2(H) (zoomed-in view of the Mayun slope showing details of GPR profile and marked cracks); yellow dotted lines represent cracks on the surface; a rose diagram shows their orientation. Panel 2(H) shows GPR profile (EF).

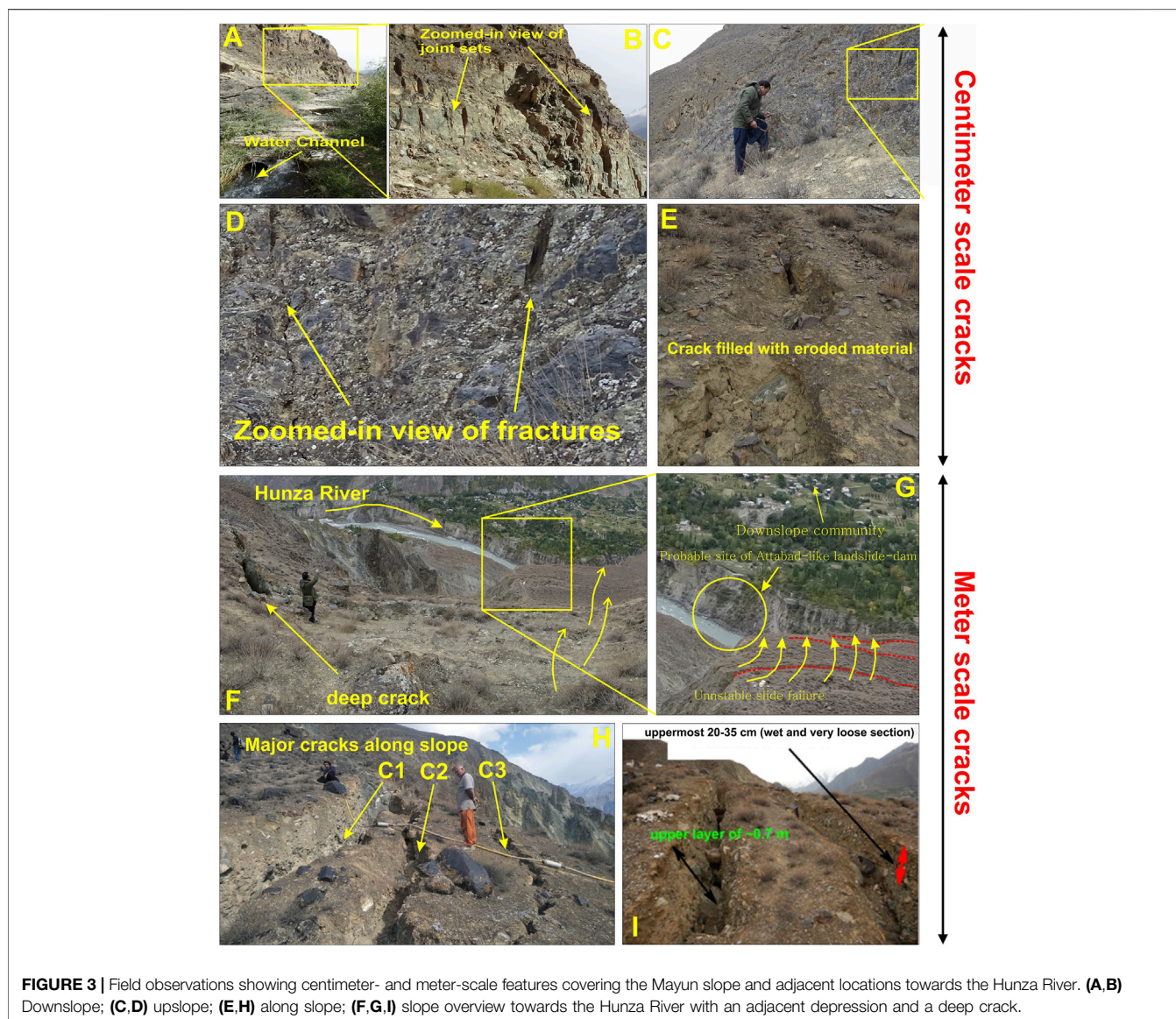


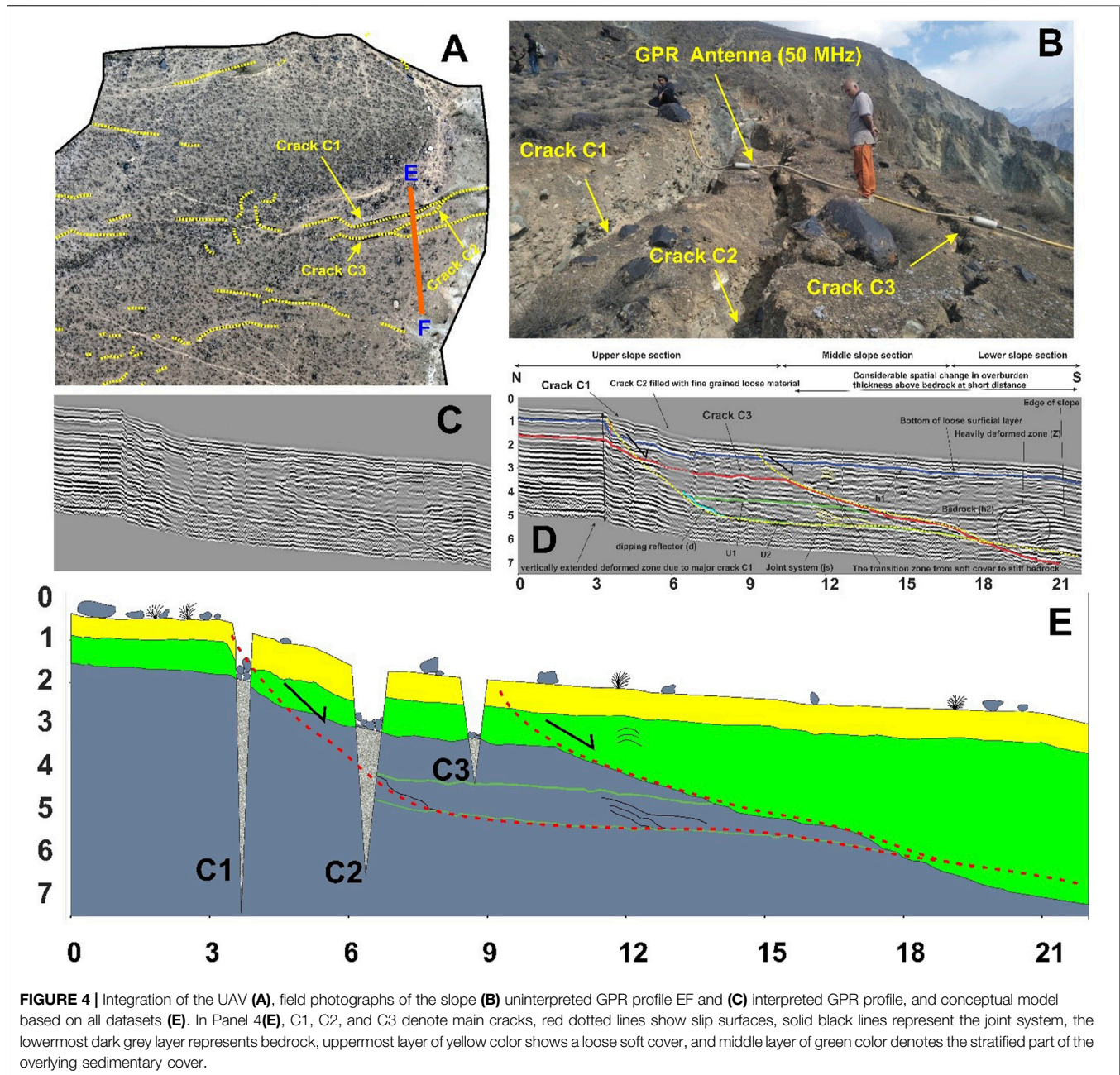
FIGURE 3 | Field observations showing centimeter- and meter-scale features covering the Mayun slope and adjacent locations towards the Hunza River. **(A,B)** Downslope; **(C,D)** upslope; **(E,H)** along slope; **(F,G,I)** slope overview towards the Hunza River with an adjacent depression and a deep crack.

of time and hence may be held responsible for reducing rock mass strength (**Figure 3A**). UAV imagery detected several zones of active erosion at the base of the rock body and the banks of the Hunza River (**Figures 2D–F**).

The texture and color differences of slope deposits assisted in the demarcation and identification of the upper, middle, and lower portions to be used in planning geophysical surveys (**Figure 2H**, see **Supplementary Figure S1**). The aerial photograph showed the varying characteristic of the slope in terms of small and large cracks and their orientation and extension mapped on its different parts. The identification of these features helped us plan the GPR experiments. Specifically, some of the GPR antenna systems (e.g., 50 MHz RTA) are specially designed for rough terrain and thus can be used at sites with rugged topography, but others (e.g., 500 MHz shielded antenna) require a ground coupling during radar data acquisition. The latter cannot be tested across the larger cracks

with meters of depth and considerable width as such large structural features disrupt the data acquisition process and may cause instrumental damage. This information was useful in selecting an appropriate radar antenna system for a particular section of the Mayun slope and hence reducing the number of GPR accessories to be transported to the remote study site. The UAV imagery with centimeters resolution captured several structural features, including three major cracks along the Mayun slope. These cracks can be easily identified due to their lateral extension (12–50 m) and width (0.3–1.2 m). The closely spaced features, filled with surficial soil and rock debris roughly striking in the roughly E–W direction, could be traced on the eastern part of the UAV map (**Figure 2C**).

At the study site, the bedrock is dominated by metamorphic rocks consisting of abundant marbles, meta-marls, and calc-silicates with subordinate metapelites and orthogneiss units (Palin et al., 2012). Field inspections showed that the bedrock



experienced intense deformation characterized by widely distributed sets of columnar joints (see **Figure 3B**). They have cut the rock mass at the study site into multiple blocks of large size with a potentially unstable nature.

The slope sections and other potential sites in the downslope area exhibited different degrees of stability and land use types. For instance, on the local road directly lying below the Mayun slope, a clear hazard from rockfall is present (**Figure 2F**). **Figure 2F** also provides such evidence where rock mass has already collapsed and the presence of a car-sized boulder on the roadside and field inspections of the deforming soft material provided a clue for a potential rockfall in the future onto the road linking Mayun to

Hussain Abad. It is important to mention that one or several processes acting simultaneously in this area of the Karakoram could trigger the movement of huge volumes of rock mass and hence result in a landslide dam (**Figures 2F, 3G**). In this context, the Attabad landslide dam is the latest example located at ~40 km upstream from the study area (**Figure 1B**).

Ground-Penetrating Radar

GPR uses electromagnetic (EM) waves (generally 10 MHz to 1,000 MHz) to image the subsurface. The radar system consists of four main units: a transmitter, receiver, control unit, and monitor. The EM energy emitted by the transmitter

is propagated downward into the ground and is reflected back due to the electrical property contrast of the subsurface layers to the ground surface, where it is collected by the receiver antenna (Khan and Rehman, 2018). This elapsed two-way travel time between the transmission and collection of the signal is measured and then used to convert the radar data to depth (Jol, 2008). Thus, a 2D image in the time or depth domain called a radargram is further processed and interpreted to extract meaningful information about the subsurface target. The detection depth depends on the antenna frequency and other factors, including signal attenuation, moisture content, and clay fractions, in the subsurface through which EM waves travel during the GPR survey (Davis and Annan, 1989). GPR data were subjected to various processing routines to reduce the noise and increase the signal-to-noise ratio.

GPR Data Collection and Results

We have employed a 50 MHz along-profile EF to delineate the downward continuation of cracks in the subsurface and dips of the fractured zones and detect bedrock depth. The flexible “snake-like” rough terrain antenna (RTA) of 50 MHz in a common-offset mode enabled us to image all sections (upper, middle, and lower) of the unstable slope and map depth of the bedrock and its internal structure (Mala, 2009), as shown in **Figure 2H**. This antenna system delivers information on specific radar signatures, representing slope properties up to several meters of depth (~8 m) with sufficient resolution. **Figure 4** reveals the subsurface structure mainly comprising overburden and bedrock with associated structural features. This migrated profile was used to pick the overburden-bedrock interface. The strong continuous reflector dipping approximately 25° to the south was interpreted as the top of bedrock with decreasing depth in the north direction. Based on geomorphologic signatures, the slope was divided into three sections (lower, middle, and upper); the latter one displayed the most damaged character compared to others. There are several radar features imaged below the bedrock, including horizontal to subhorizontal dipping (d), joint system (js) roughly dipping in the direction of slope, and a few other doubtful and unsystematic discontinuities with no defined reflection configuration. In addition, we detected two continuous horizontal reflections (U1 and U2) traceable throughout the georadar section underneath the high-amplitude bedrock interface (h2). These two features most probably resulted from a considerable lithological change or bedrock foliation. The deformed zone beneath crack C3 extends to the top of the U1, which is further connected through the dipping reflector (d), marked as a solid cyan line, to the deformed zone beneath crack C2 (**Figure 4D**). This suggests connectivity of the aforementioned deformed zones and thus of C2 and C3 in the subsurface. The radar signature U2 is relatively weak and less coherent due to increased depth. However, the influence of disruption/offsetting of reflection events caused by major cracks can be seen on both reflectors (U1 and U2). This provides evidence of fractured bedrock recognized on the GPR section (**Figure 4**). Moreover, the presence of the joint

system on the radar section supported by field observations suggested that the internal structure of bedrock is heavily deformed.

The high-resolution bedrock reflection approaches the surface at the northern edge of the radar cross-section. A site-specific decrease in its depth and slope angle was observed in the bedrock's surface underneath 15 m. Heading south along the GPR profile (**Figure 4**), the reflector h2 was coherent and could be easily followed all the way down from 10 to 17 m to a maximum depth of approximately 7.6 m along the GPR transect. It is relatively difficult to pick the bedrock reflector in the northern part due to extended deformation induced by three major cracks (C1, C2, and C3). Besides the disrupted subsurface structure in the upper slope, the wet and highly heterogeneous nature of the topmost part of the first layer (h1), bedrock morphology, and low-frequency GPR data were among the possible factors limiting the chances of tracing the bedrock at shallow depths. The most heavily deformed zone (z) within the overburden was one of the prominent features due to its considerable lateral and vertical dimension, horizontal to subhorizontal reflections, offsetting of reflectors with few unlikely events and/or diffractions. Several radar signatures of structural importance within this lowermost slope section were attributed to part of the unstable compartment adjacent to the valley side, the maximum thickness of overburden, and almost detached blocks. Such features are making the lower part of the slope more susceptible to generate slope instabilities. We were able to map three major cracks in the upper section of the unstable slope. A continuous decrease in the width and slip can be noticed in an N-S direction along deeply propagating major cracks. The correlation between geomorphologic observations in the field with high-resolution radar images confirms their vertical continuation and spatial distribution in the subsurface. The offset reflection boundaries along the marked interfaces in the subsurface exhibit the sliding direction towards the south, which is normal to the E-W-oriented main deformation along the Mayun unstable slope and the trace of the Main MKT. GPR-based results supported by geomorphological observations suggest a stress regime of a complex tectono-geomorphological setting. The literature has also shown the role of regional tectonic features (e.g., MKT fault) in the activity of unstable slopes like the one under investigation in the Karakoram Himalaya (Dini et al., 2019).

Figure 4 shows the lower contact of a stratified layer that contains little to no deformation in the middle section but lateral continuity along the transect. We observed no inclined reflections or layers and other features within this geological unit except the northern part, where chaotic and discontinuous reflections represent crack-induced deformation structures. The appearance of deformation structures at various depths (i.e., detection of underground cracks, joint sets, spatial variation in thickness of overburden, and demarcation of more or less horizontal stratigraphic layers on high-resolution radar image) demonstrates the inter-play between deposition, tectonic deformation, and erosion.

The geological boundaries, h1 and h2, separate the topmost loose deposits from a relatively stratified cover of the soft cover and the soft cover from the bedrock, respectively. The radar signatures also show deeply propagating cracks filled with weathered material, their slip, dimension, and depth distribution, consistent with the field evidence (Figure 4B). All these features explain the internal structure of overburden, depth of the unstable slope, and associated deformation patterns in soft deposits and bedrock. Among other factors, this information is critical for an improved understanding of slope dynamics and, with a reasonable degree of certainty, is considered a prerequisite in slope stability analyses (Hack, 2000).

DISCUSSION

This section presents the integration of different datasets and their implications for slope dynamics. High-resolution radar profiles covering relatively stable locations showed a number of discontinuities in the very shallow subsurface. The combined geomorphological mapping, aerial photographs, and geophysical measurements have provided an insight into the structural features of the overburden and complex internal structure of the unstable slope (Figure 4). The remote sensing imagery identified large-scale features around the Mayun slope and in the downslope area (Figure 2). The stratigraphic layers estimated from the GPR measurements, less deformed character of h1 and h2 reflectors, and increased thickness of the overburden underneath the middle slope section suggest its stable nature compared to other parts. These results were found in agreement with the field observations. GPR depth section showed two overburden layers (soft surficial and stratified) and a compact metamorphic bedrock. The depth of dipping bedrock varied from 1.6 to 7.5 m in an N-S direction. The GPR profile of the 50 MHz antenna delineated thickness variation of loose deposits in the downslope direction with maximum and minimum values of about 7.5 and 1.6 m. The deeper slope structure revealed by three radar features based on a change in the radar reflections includes a dipping reflector connecting two main cracks C2 and C3, subhorizontal radar signatures depicting a set of joints, and horizontal reflections of continuous character probably resulting from a considerable lithological change or bedrock foliation. The foliations may provide planes of weakness that subsequently may result in slip surfaces. Likewise, the subsurface radar-derived joint system supported by the outcrop data suggests the jointed, and hence potentially, unstable nature of the bedrock at the Mayun slope (see Figures 3B, 4D). The relationship between the joint systems and the slope has been reported in the literature to demonstrate its impacts on slope stability (Li et al., 2020). The radar data further showed deep cracks running through bedrock, which agree with the deformation patterns of outcropped section at the subject site. The delineation of slip surface(s) in slope studies in high mountainous regions has always been a complicated task

due to their existence at different depths, local structures/instabilities, diversity of topography, extremely heterogeneous surficial deposit of deformed character, and significant variations in moisture content, which restrict the efficient use of geophysical surveys. However, combining geophysical results with field observations could help identify the slip surface(s). Our work documents this using *in situ* slip signatures extending from the bottom of the main cracks, which was further confirmed through the GPR record (Figures 4B,D,E). This result highlights the importance of the combined use of field surveys and remote sensing technologies. The configuration and significant displacement along major cracks in the field and offset of radar reflections in the sheared zone (~5–10 m) assisted our interpretation by tracking the two possible slip surfaces and finally constructing the conceptual model (Figures 4D,E).

The weathered surficial deposits and field evidence of structural features at multiple locations confirms the radar-derived results (Figure 4). The length and number of radar profiles were limited by the available time, financial support, and rugged topography of the remote site. It can be seen that the spatial variation of the interpreted thickness of soft surficial strata and its varying degree of stability have significantly influenced slope stability along its different sections at the subject site. Extra complexity reflected by almost detached blocks and meter-scale disruption of material due to deep cracks may ultimately lead to potential slope failure (Figures 2, 4B).

CONCLUSION

The UAV-based mapping proved to be an effective and low-cost tool for revealing the major geomorphic features of an unstable slope. The aerial photos assisted in planning geophysical surveys and obtaining a larger picture of its adjacent area in the downslope direction. High-resolution GPR data provided information on the debris cover thickness, deformation patterns, and stratigraphic contacts at shallow and medium depths. The 50 MHz RTA profile mapped the overburden and the internal structure of bedrock by revealing joint systems, well-defined reflections related to cracks and their depth distribution, the interconnectivity of cracks in the subsurface, and sheared zones. The major cracks were found cutting through the entire slope structure and causing a considerable disruption of the reflectors in the crest section. Such open cracks contribute to the deep weathering of bedrock by exposing them to water inflow. The field evidence aided the interpretation of possible slip surfaces on the radargram at shallow and relatively large depths, highlighting the full potency of GPR in investigating the slope dynamics.

The Mayun slope appears to be unstable, putting the Mayun village and a section of the KKH at a severe landslide risk in the future, especially if there is a moderate-to-large size earthquake. Therefore, further detailed investigation and monitoring should be implemented on a priority basis to understand the triggering mechanism and assist in the risk reduction in an area subjected to potential geohazards.

DATA AVAILABILITY STATEMENT

The original contributions presented in the study are included in the article/**Supplementary Material**; further inquiries can be directed to the corresponding author.

ETHICS STATEMENT

Written informed consent was obtained from the relevant individual(s) for the publication of any potentially identifiable images or data included in this article.

AUTHOR CONTRIBUTIONS

MYK collected and processed the GPR data. MS performed the UAV data analysis and interpretation. SAT collected and interpreted geological data, and prepared most of the figures.

REFERENCES

- Alvarez, W. (2010). Protracted continental Collisions Argue for continental Plates Driven by Basal Traction. *Earth Planet. Sci. Lett.* 296, 434–442. doi:10.1016/j.epsl.2010.05.030
- Ballantyne, C. K. (2002). Paraglacial Geomorphology. *Quat. Sci. Rev.* 21, 18–19. doi:10.1016/S0277-3791(02)00005-7
- Bird, J. F., and Bommer, J. J. (2004). Earthquake Losses Due to Ground Failure. *Eng. Geology* 75, 147–179. doi:10.1016/j.enggeo.2004.05.006
- Bürkle, A., Segor, F., and Kollmann, M. (2011). Towards Autonomous Micro UAV Swarms. *J. Intell. Robot Syst.* 61, 339–353. doi:10.1007/s10846-010-9492-x
- Chen, X., Cui, P., You, Y., Cheng, Z., Khan, A., Ye, C., et al. (2017). Dam-break Risk Analysis of the Attabad Landslide Dam in Pakistan and Emergency Countermeasures. *Landslides* 14, 675–683. doi:10.1007/s10346-016-0721-7
- Crawford, M. B., and Searle, M. P. (1993). *Collision-related Granitoid Magmatism and Crustal Structure of the Hunza Karakoram*, 74. North Pakistan: Geological Society, Special Publications, 53–68. doi:10.1144/gsl.sp.1993.074.01.05
- Cronin, V. S., Maliniconico, L. L. A., and Lillie, R. J. (1989). “Structural Setting of the Skardu Intermontane basin, Karkoram Himalaya, Pakistan,” in *Tectonics and Geophysics of the Western Himalaya* (America: Geological Society, Special Paper), 232, 183–202. doi:10.1130/spe232-p183
- Danneels, G., Bourdeau, C., Torgoev, I., and Havenith, H.-B. (2008). Geophysical Investigation and Dynamic Modelling of Unstable Slopes: Case-Study of Kainama (Kyrgyzstan). *Geophys. J. Int.* 175, 17–34. doi:10.1111/j.1365-246X.2008.03873.10.x
- Davis, J. L., and Annan, A. P. (1989). Ground-penetrating Radar for High-Resolution Mapping of Soil and Rock Stratigraphy. *Geophys. Prospect.* 37, 531–551. doi:10.1111/j.1365-2478.1989.10.1111/j.1365-2478.1989.tb02221.x
- De Filippi, F. (1912). *Karakoram and Western Tibet, 1909*. London.
- Deparis, J., Fricout, B., Jongmans, D., Villemin, T., Effendiant, L., and Mathy, A. (2008). Combined use of geophysical methods and remote techniques for characterizing the fracture network of a potentially unstable cliff site (the ‘Roche du Midi’, Vercors massif, France). *J. Geophys. Eng.* 5, 147–157. doi:10.1088/1742-2132/5/2/002
- Deparis, J., Garambois, S., and Hantz, D. (2007). On the potential of Ground Penetrating Radar to help rock fall hazard assessment: A case study of a limestone slab, Gorges de la Bourne (French Alps). *Eng. Geology* 94, 89–102. doi:10.1016/j.enggeo.2007.07.005
- Dini, B., Manconi, A., and Loew, S. (2019). Investigation of Slope Instabilities in NW Bhutan as Derived from Systematic DInSAR Analyses. *Eng. Geology* 259, 105111–111. doi:10.1016/j.enggeo.2019.04.008
- NA collected UAV data, contributed to the UAV data processing. MYK wrote the manuscript, with contributions from SAT and MS. All authors contributed to the discussion of the results and revisions of the manuscript.
- Fan, X., Xu, Q., Scaringi, G., Dai, L., Li, W., Dong, X., et al. (2017). Failure Mechanism and Kinematics of the Deadly June 24th 2017 Xinmo Landslide, Maoxian, Sichuan, China. *Landslides* 14 (6), 2129–2146. doi:10.1007/s10346-017-0907-7
- Fey, C., and Wichmann, V. (2017). Long-range Terrestrial Laser Scanning for Geomorphological Change Detection in alpine Terrain - Handling Uncertainties. *Earth Surf. Process. Landforms* 42, 789–802. doi:10.1002/esp.4022
- Ghorbanzadeh, O., Meena, S. R., Blaschke, T., and Aryal, J. (2019). UAV-based Slope Failure Detection Using Deep-Learning Convolutional Neural Networks. *Remote Sensing* 11, 2046–46. doi:10.3390/rs11172046
- Goudie, A. S., Brunsdon, D., Collins, D. N., Derbyshire, E., Ferguson, R. J., Jones, D. K. C., et al. (1984). “The Geomorphology of the Hunza Valley, Karakoram Mountains, Pakistan: Project 2,” in *The International Karakoram* (Cambridge), 359–410.
- Hack, R. (2000). Geophysics for Slope Stability. *Surv. Geophys.* 21, 423–448. doi:10.1023/a:1006797126800
- Hewitt, K. (2001). Catastrophic Rockslides and the Geomorphology of the Hunza and Gilgit River Valleys, Karakoram Himalaya. *erdkunde* 55, 72–93. doi:10.3112/erdkunde.2001.01.05
- Hewitt, K., Gosse, J., and Clague, J. J. (2011). Rock Avalanches and the Pace of Late Quaternary Development of River Valleys in the Karakoram Himalaya. *Geol. Soc. America Bull.* 123, 1836–1850. doi:10.1130/B30341.1
- Holmes, J. A., and shroder, J. F. (1993). “Present and Past Patterns of Glaciation in the Northwest Himalaya: Climatic, Tectonic and Topographic Controls,” in *Himalaya to the Sea: Geology, Geomorphology and the Quaternary* (New York, 72–90.
- Huang, H., Long, J., Lin, H., Zhang, L., Yi, W., and Lei, B. (2017). Unmanned Aerial Vehicle Based Remote Sensing Method for Monitoring a Steep Mountainous Slope in the Three Gorges Reservoir, China. *Earth. Sci. Inform.* 10, 287–301. doi:10.1007/s12145-017-0291-9
- Jol, H. M. (2008). *Ground Penetrating Radar Theory and Applications*. Amsterdam: Elsevier.
- Khan, M. Y., and Rehman, K. (2018). Non-destructive Assessment of a Destructive Forensic Scene, an Example of Emerging Geophysical Technology in Applied Criminology. *J. Himalayan. Earth. Sci.* 52, 2019.
- Khan, M. Y., Turab, S. A., Riaz, M. S., Atekwana, E. A., Muhammad, S., Butt, N. A., et al. (2021). Investigation of Coseismic Liquefaction-induced Ground Deformation Associated with the 2019 M W 5.8 Mirpur, Pakistan, Earthquake Using Near-surface Electrical Resistivity Tomography and Geological Data. *Near Surf. Geophys.* 19, 169–182. doi:10.1002/nsg.12148
- Li, H.-b., Qi, S.-c., Yang, X.-g., Li, X.-w., and Zhou, J.-w. (2020). Geological Survey and Unstable Rock Block Movement Monitoring of a post-earthquake High

FUNDING

The authors have conducted the fieldwork using the financial support of the Higher Education Commission, Pakistan (HEC). Unfortunately, they do not have additional funds to pay the charges for this manuscript.

SUPPLEMENTARY MATERIAL

The Supplementary Material for this article can be found online at: <https://www.frontiersin.org/articles/10.3389/feart.2021.668011/full#supplementary-material>

- Rock Slope Using Terrestrial Laser Scanning. *Rock. Mech. Rock. Eng.* 53, 4523–4537. doi:10.1007/s00603-020-02178-0
- Mala (2009). *ProEx—professional Explorer Control Unit. Operating Manual*. Malå, Sweden: Mala, 60.
- Marescot, L., Monnet, R., and Chapellier, D. (2008). Resistivity and Induced Polarization Surveys for Slope Instability Studies in the Swiss Alps. *Eng. Geology* 98, 18–28. doi:10.1016/j.enggeo.2008.01.010
- Marsella, M., D'Aranno, P. J. V., Scifoni, S., Sonnessa, A., and Corsetti, M. (2015). Terrestrial Laser Scanning Survey in Support of Unstable Slopes Analysis: the Case of Vulcano Island (Italy). *Nat. Hazards* 78, 443–459. doi:10.1007/s11069-015-1729-3
- Palin, R. M., Searle, M. P., Waters, D. J., Horstwood, M. S. A., and Parrish, R. R. (2012). Combined Thermobarometry and Geochronology of Peraluminous Metapelites from the Karakoram Metamorphic Complex, North Pakistan; New Insight into the Tectonothermal Evolution of the Baltoro and Hunza Valley Regions. *J. Metamorph. Geol.* 30, 793–820. doi:10.1111/j.1525-1314.2012.00999.1.1111/j.1525-1314.2012.00999.x
- Petschko, H., Bell, R., and Glade, T. (2016). Effectiveness of Visually Analyzing LiDAR DTM Derivatives for Earth and Debris Slide Inventory Mapping for Statistical Susceptibility Modeling. *Landslides* 13, 857–872. doi:10.1007/s10346-015-0622-1
- Roque, D., Perissin, D., Falcão, A. P., Amado, C., Lemos, J. V., and Fonseca, A. M. (2018). Analysis of InSAR Displacements for the Slopes Around Odelouca Reservoir. *Proced. Comp. Sci.* 138, 338–345. doi:10.1016/j.procs.2018.10.048
- Seeber, L., and Gornitz, V. (1983). River Profiles along the Himalayan Arc as Indicators of Active Tectonics. *Tectonophysics* 92, 335–367. doi:10.1016/0040-1951(83)90201-9
- Shafique, M., Khan, M. Y., Rahman, A. U., Khan, A. N., and Shaw, R. (2015). “Earthquake Hazards and Risk Mitigation in Pakistan,” in *Disaster Risk Reduction Approaches in Pakistan* (Japan: Springer Tokyo), 101–117. doi:10.1007/978-4-431-55369-4_5
- Shroder, J. F., Owen, L. A., and Derbyshire, E. (1993). “Quaternary Glaciation of the Karakoram and Nanga Parbat Himalaya” in: *Himalaya to the Sea: Geology, Geomorphology and the Quaternary*. New York, 132–158.
- Tahar, K. N. (2012). A New Approach on Slope Data Acquisition Using Unmanned Aerial Vehicle. *Intern. J. Res. Rev. Appl. Sci.* 13, 780–785.
- Toshioka, T., Tsuchida, T., and Sasahara, K. (1995). Application of GPR to Detecting and Mapping Cracks in Rock Slopes. *J. Appl. Geophys.* 33, 119–124. doi:10.1016/0926-9851(95)90035-7
- Willenberg, H., Eberhardt, E., Evans, K. F., Heincke, B., Maure, H., Loew, S., et al. (2018). Internal Structure and Deformation of an Unstable Crystalline Rock Mass above Randa (Switzerland), from Integrated Geological and Geophysical Investigations. *J. Maps* 101, 1–14. doi:10.1016/j.enggeo.2008.01.015
- Zeitler, P. K. (1985). Cooling History of the NW Himalaya, Pakistan. *Tectonics* 4, 127–151. doi:10.1029/TC004i001p00127

Conflict of Interest: The authors declare that the research was conducted in the absence of any commercial or financial relationships that could be construed as a potential conflict of interest.

Publisher's Note: All claims expressed in this article are solely those of the authors and do not necessarily represent those of their affiliated organizations, or those of the publisher, the editors and the reviewers. Any product that may be evaluated in this article, or claim that may be made by its manufacturer, is not guaranteed or endorsed by the publisher.

Copyright © 2021 Khan, Shafique, Turab and Ahmad. This is an open-access article distributed under the terms of the Creative Commons Attribution License (CC BY). The use, distribution or reproduction in other forums is permitted, provided the original author(s) and the copyright owner(s) are credited and that the original publication in this journal is cited, in accordance with accepted academic practice. No use, distribution or reproduction is permitted which does not comply with these terms.